NATURALISTA CAMPANO
ISSN: 1827-7160
Volume 28 Issue 1, 2024

Synthesis of Chitosan Nanoascorbate Bombyx Mori

Kudrat Pirniyazov[1], I'lnar Nurgaliev[2*], Sayyora Rashidova[3]
[1,2*,3]Institute of polymer chemistry and physics, Academy of Sciences of the Republic of Uzbekistan, Tashkent, Uzbekistan
[1]Corresponding Email: [2*]qudrat.pirniyazov@mail.ru

Abstract. In the present work, chitosan nanoascorbate Bombyx mori (CSNA) based on high-molecular-weight chitosan (CS) and ascorbic acid (AA) was synthesized by ionotropic gelation in the presence of tripolyphosphate (TPP). The results of the conducted kinetic studies show that in the studied interaction, the order of the reaction of ascorbic acid exceeds the order of the reaction of chitosan. In this study, theoretical studies based on density functional theory (DFT) have performed to comprehend the interaction between of chitosan dimer with AA and sodium tripolyphosphate (TPP) by during the formation of chitosan ascorbate (CSA) nanostructure. Based on existing results, the CS monomer formed of complexes occurs due to the donor-acceptor interaction, which is energetically favorable in all considered inter-actions according to the calculations. The order of values interaction energy de-creases: CS-AA (-68.76 kcal/mol), CS-TPP (-64.58 kcal/mol), which indicates that in the process of formation of CSNA, in most cases, the formation of a donor-acceptor bond occurs between the amino groups of CS with the enol group of AA. The introduction of the aqueous phase led to a drop in the interaction energy. CS nanoparticles can protect ascorbic acid from degradation and improve the stability of AA.

Keywords: Chitosan; Chitosan Nanoascorbate, Ascorbic Acid; Donor-Acceptor Bond; Reaction Rate; Density Functional Theory.

1. Introduction

Chitosan (CS), the deacetylated product of chitin, is a polysaccharide consisting of N-acetyl-D-glucosamine and D-glucosamine linked by the β-(1→4) bonds [1]. Ascorbic acid (AA) is known to play an important role in metabolism, acting as both an acceptor and a proton donor in enzymatic systems, due to the mobility of hydrogen atoms in enol hydroxyls at C-3 (pKa = 4.2) and C-2 (pKa = 11.6). CS is biodegradable, nontoxic biopolymer, has properties stimulates plant growth, and inhibits phytopathogenic fungi [1, 2]. Of great interest in the world are water-soluble, environmentally safe derivatives of CS, in particular, CS ascorbate (CSA). A wide possibility of CS modification allows to obtain its water-soluble derivatives, among which ACS is of special interest, which exhibits pronounced bioactivity in the growth and development of plants [2-4].

The use and study of the physicochemical properties of biologically active nanostructured complexes of CS with organic acids is poorly understood, and there are few works on determining the activation energy of the formation reaction and modeling the structure of CS nanoascorbate (CSNA) [1]. Complexes of CS with organic acids are obtained mainly by the method of ionotropic gelation, coacervation precipitation and ultrasonic dispersion. However, there are advantages and disadvantages of the above methods for obtaining nanoparticles. If the method of ionotropic gelation is considered technologically acceptable and no additional purification is required for a long time of the final products, then by the method of coacervation precipitation, side compounds are formed due to ions of inorganic salts. When obtaining nanoparticles of CS derivatives by ultrasonic dispersion, it is impossible to control the process, which in turn makes it difficult to control their characteristics.

Thus, the formation of nanoparticles is a multifactorial process that depends on the ratio, concentration of components, and solution pH [2, 3]. Among the methods for obtaining CSNA, the method of ionic gelation is the most well-known, however, in studies when obtaining CSNA, deprotonation of CS is not carried out; this stage plays a special role in the formation of a donor-acceptor bond between the amino group of CS and the enol group of AA [4-6]. Since without deprotonation of the amino groups of CS, an excess amount of AA in the reaction system increases, which makes it impossible to analyze the properties of the final product [2, 3, 7].

Therefore, in this work, we improved the method with the inclusion of the step of deprotonation of CS amino groups. Based on the obtained deprotonated CS with varying pH and the ratio of the reaction components and the TPP stabilizer, it is possible to control the size of the resulting nanoparticles of CS derivatives with organic acids, including AA [4–6]. Nano derivatives of CS with AA have growth-regulating, antimicrobial, and wound-healing properties; solutions of nano derivatives of CS are low-toxic and environmentally safe, have

antimicrobial, growth-stimulating properties, and can reduce the susceptibility to root rot in comparison with the standard and untreated seeds [8-13]. It is noted in the literature that the reaction of formation of CSNA occurs due to the donor-acceptor bond. The ratio of components and solution pH play a special role in this process [13, 14]. In order to obtain water-soluble nano-derivatives of CS, aqueous solutions of AA are used. The formation of CSNA is carried out by varying the pH of the solution in the range from 4 to 5.5 [15, 16].
CA is an organic salt formed by the reaction of CS with AA and it shows a more pH-independent solubility profile, thus providing more flexibility in biomaterial processing and fabrication. CA is synthesized by the direct reaction of CS and AA in water (Figure 1) [7-9].

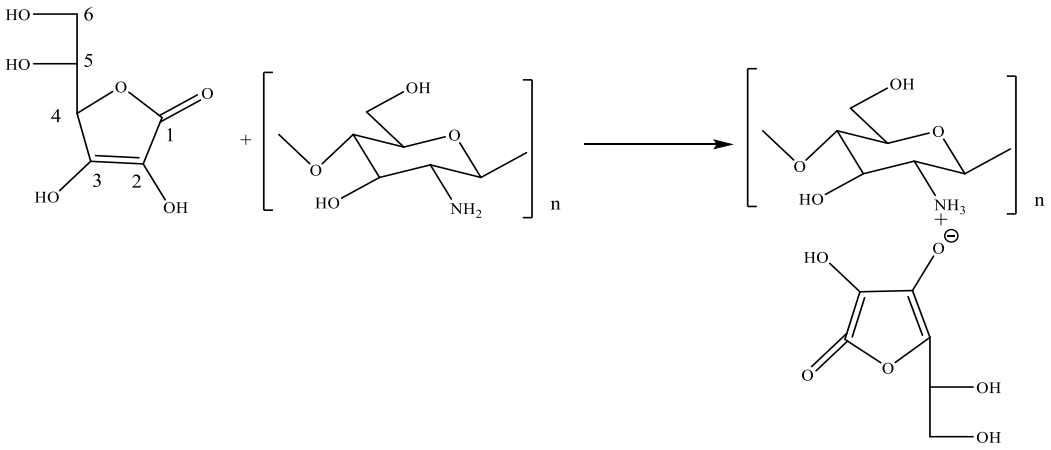

Figure 1**.** Mechanism of interaction between CS and AA.

The use and study of the physicochemical properties of biologically active nanostructured complexes of CS with organic acids are poorly studied, and scientific works on determining the reaction order of formation of CSNA have not been found [2, 14–17]. For this purpose, CSNA based on Bombyx mori CS was obtained for the first time and the physicochemical properties of nanostructural complexes of CS with AA were studied. Based on the foregoing, in this work we carried out the synthesis, quantum chemical modeling of the structure, and evaluation of the physicochemical properties of CSNA.

2. Materials And Methods

Determination of the molecular weight of the initial chitosan
In this work, we used high-molecular-weight CS with a molecular weight of 101 kDa and a degree of deacetylation (DD) of 84 %, obtained from the pupae of the silkworm Bombyx mori. Aqueous solutions of 0.3 M acetic acid were used as a solvent, while the concentration of the initial CS was 0.5 %. The outflow time of the solution (t) and solvent (t_0) was experimentally determined, then the viscosity ratio (η/η_0), specific viscosity $\eta_{sv}= (\eta- \eta_0)/\eta_0$, and viscosity number $\eta_{sn}/C= (\eta- \eta_0)/\eta_0 C$ were determined. The intrinsic viscosity of CS solutions was determined at a temperature of 303.15 ± 0.05 K in a solution of 0.3 M CH_3COOH + 0.3 M CH_3COONa. Experimentally, the intrinsic viscosity was determined by double graphical extrapolation of the values η_{sv}/C and $\ln(\eta_{rel}/C)$ to zero concentration. In this case, linear dependences of the reduced viscosity η_{sp}/C on concentration are obtained, which are described by the Huggins equations:

$$\eta_{sv/c} =[\eta]+K_x[\eta]^2\times C \qquad (1)$$

The molecular weight is determined according to the formula

$$[\eta] = 1.41 \times 10\text{-}4 \times M\eta^{0.83} \qquad (2)$$

Determination of the degree of deacetylation of chitosan
The DD of the initial CS was determined by conductometric titration on a Metler Tolledo automatic titrator in a 0.1 N solvent. of hydrochloric acid. At the same time, the prepared 1% CS solution was titrated with a 0.5 M NaOH solution. The degree of deacetylation of CS is determined by the formula:

$$DD = 203,3\times100/(42+1000\times m_0/C_{NaOH}\times V_{NaOH}) \qquad (2.2.1.)$$

where: 203.3; 42; 100; 1000 - calculated coefficients; m - sample CS; V is the volume of consumed NaOH titrant, mL; C, NaOH is the concentration of NaOH.

Structural studies

The structural characteristics of the obtained CSNA were studied by IR spectroscopy on an IR Bruker spectrometer (Germany). To study the particle sizes of the obtained samples, AFM studies were performed using an Agilent 5500 atomic force microscope.

Synthesis of chitosan nanoascorbate and determination of kinetic parameters

The reaction of the formation of CSNA was carried out by the method of ionotropic gelation with varying the ratio of components - CS and AA, the pH of the solution, at a temperature of 20 to 50^0C. A 0.5% TPP solution was used as a nanoparticle stabilizer, since it is non-toxic, and this approach is technologically efficient. Ethyl alcohol (chemically pure) was used as a precipitant. To estimate the reaction order, the dependence of the logarithm of the rate of the reaction for the formation of CSA nanoparticles on the concentrations of the initial CS and AA was plotted.

Quantum-chemical modeling of the structure

Model of interaction of monomer form of CS with AA and TPP were built. All the studied models were computed by the GAUSSIAN09 program [18]. Studied models were optimized with DFT theory at the B3LYP/ 6-31++G (d,p) [19-22]. The first stage of the calculation was the determination of the optimized molecular structures of CS and AA. The charge state of atoms has been calculated, diagrams of boundary molecular orbitals have been constructed: the highest occupied (HOMO) and lowest free (LUMO) molecular orbitals, and their energies have been determined. In DFT reactivity descriptors, such as global hardness (η) is defined using finite difference approximation and Koopmans' theorem [23-25] as: $\eta = \frac{1}{2}\left(\frac{\partial^2 E}{\partial N^2}\right)_{\upsilon(\vec{r})} = \frac{1}{2}\left(\frac{\partial \mu}{\partial N}\right)_{\upsilon(\vec{r})}$,, where E is the energy and N is the number of electrons in the electronic system at constant external potential (υ), μ is the chemical potential ($\mu = 1/2(E_{HOMO} + E_{LUMO})$), η was be calculated in terms of ionization potential ($-E_{HOMO}$) and electron affinity ($-E_{LUMO}$) using the following formulae: $\eta=(E_{LUMO}-E_{HOMO})/2$.

Free energy of solvation is computed by equation: $\Delta G_{sol} = G_{solvent} - G_{gas}$, that numerical values obtained by using SMD solvation model [26]. Strength of hydrogen bonding is expressed in terms of interaction energy (ΔE_{int}) which is calculated using super molecular approach [for $CS + AA \rightarrow CS - AA$ and $CS + TPP \rightarrow CS - TPP$, $\Delta E_{int} = E_{CS-AA} - (E_{CS} + E_{AA})$, $\Delta E_{int} = E_{CS-TPP} - (E_{CS} + E_{TPP})$, where, E is the total energy of the molecules. Global reactivity descriptor namely the global hardness is calculated using global hardness values. In order to quantify the reactivity in aqueous phase, solvation energies are calculated using self-consistent reaction field theory using Polarizable Continuum Model (PCM) [27, 28]. In calculating interaction energy, basis set superposition error (BSSE) is taken into account by using counterpoise = N [29, 30].

3. Results And Discussion

By varying the concentration of the initial components, the order of the reaction, the yield of final products, and the degree of binding of CS with AA were determined. At a constant concentration of AA, with an increase in the concentration of CS, the degree of AA binding and the yield of end products increase. Also, with an increase in the ratio of CS, an increase in the reaction rate is found. The results obtained are presented in Table 1.

Table 1. Dependence of the degree of binding (DB) of CS with AA and the rate of the reaction of formation of CSNA on the concentration of CS (t=30 ^{0}C, τ= 15 minutes). The initial concentration of AA 0.1 mol/L.

CS, mol/L	AA, ΔC^*, mol/L	DB, %	Yield, %	Reaction speed· 10^{-5} mol/L.s.
0,025	0,045	45,0	57,0	5,0
0,05	0,060	60,0	59,0	6,7
0,1	0,082	82,0	67,0	8,9
0,2	0,087	87,8	69,7	9,7
0,3	0,090	90,0	77,8	10,0
0,4	0,093	93,0	87,5	10,3

As can be seen from the results obtained, with a ratio of components of CS:AA 0.025:0.1, the excess amount of AA is on average 55 %. The rest of the AA interacts with CS and is partially neutralized by sodium ions formed due to the dissolution of the TPP salt. Further, with an increase in the concentration of CS, a regular increase in the content of AA in the composition of CSNA was found. The same results of the reaction at a constant concentration of CS (0.5 mol/L) - with an increase in the ratio of AA, a regular increase in the reaction rate and the content of AA in the composition of CSNA occurs. However, with the establishment of an equivalent ratio of the components of CS:AA 1:1, there is a decrease in the degree of binding of AA due to its excess amount. The results obtained are presented in Table 2. As can be seen from the data obtained, with an increase in the ratio of components more than 1:1, the reaction rate remains practically constant. The order of the CSNA formation reaction was estimated and the dependence of the logarithm of the reaction rate on the concentrations of the initial CS and AA was plotted. According to the tangent of the slope angle, the values of the reaction orders for CS and AA were determined, which are equal to 0.5–0.9, indicating that with an increase in the concentration of AA compared to CS, the reaction rate almost doubled.

Table 2. Dependence of the degree of binding (DB) of AA and the rate of the reaction of formation of CSNA on the concentration of AA (t=30^{0}C, τ=15 minutes). CS concentration (0.5 mol/L.).

AA, mol/L	AA, ΔC, mol/L	DB, %	Yield, %	Reaction rate, 10^{-4} mol/L.s.
0,2	0,18	94,0	82,8	2,10
0,3	0,27	91,0	71,3	3,07
0,5	0,43	85,6	66,5	4,77
1,0	0,45	42,0	41,2	4,67

Previously, it was shown [4, 16] that in the formation of CSA from high-molecular-weight CS at a concentration of 0.2 (0.5), the reaction order in terms of the concentration of the initial CS was 0.76. CSNA is stabilized by TPP, therefore, part of the amino groups are blocked and Therefore, the formation reaction rate and the order in CS are somewhat lower than in the case of unstabilized CS due to the relatively low concentration of amino groups available for interaction.

4. RESULTS OF AFM STUDIES

It has been established that by varying the ratio of the components of CS: AA and the concentration of the stabilizer - TPP, it is possible to control the size of the CSNA particles, a 0.5% solution of the stabilizer in the formation of CSNA is optimal. The structural characteristics and particle sizes of the obtained samples of CSNA Bombyx mori were determined. The particle sizes of the obtained samples are in the range of 16-100 nanometers (Figure 2).

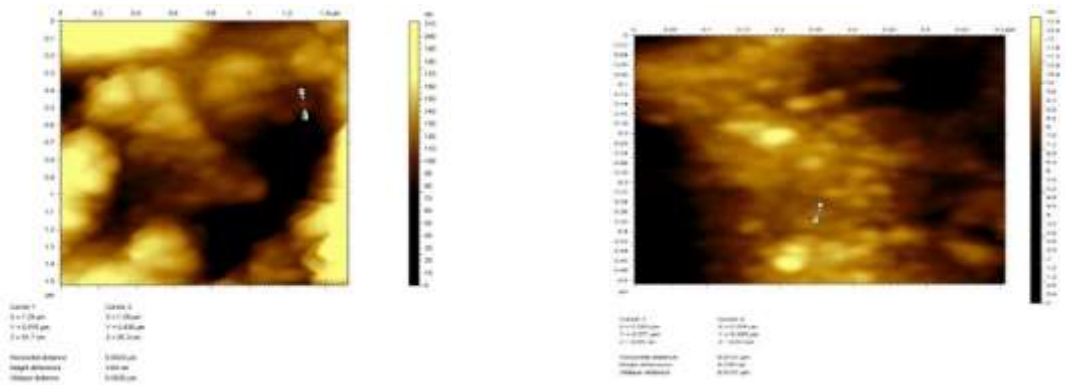

Figure 2. a) AFM images of CSNA in the ratio of components CS:AA:TPP 4:1:0.5
b) AFM images of CSNA in the ratio of components CS:AA:TPP 4:1:0.25.

The obtained results confirm that in the range of component ratios of CS:AA:TPP 4:1:0.5 - 4:1:0.25, a high yield of end products was found and the sizes of nanoparticles are in the range of 16 - 100 nanometers, respectively.

Results of IR spectroscopic studies. In the IR spectrum of CS, all characteristic absorption bands corresponding to the CS structure were found. Thus, at 1670 and 1600 cm^{-1}, absorption bands corresponding to the functional groups of acetamide (amide I) and amine were found [13]. In the AA spectra in the range of 3200-2900 cm^{-1} there are absorption bands of stretching vibrations of C2 and C3 of hydroxyl groups, and in the range of 2915-2900 cm^{-1} - for the methylene group. At 1750 cm^{-1}, an absorption band is found for the carbonyl group included in the lactone ring of AA; at 1600 cm^{-1} absorption band characteristic of C=C groups. In the IR spectra of the obtained CSNA, absorption bands appear that differ from the absorption bands of CS and AA. There is a shift of the absorption bands corresponding to the functional groups of acetamide and amine towards lower wave numbers from 1600 to 1540 cm^{-1}, which indicates the formation of a CS derivative - CSNA. In the region of 1400–900 cm^{-1}, absorption bands characteristic of CS appear (Figure 3).

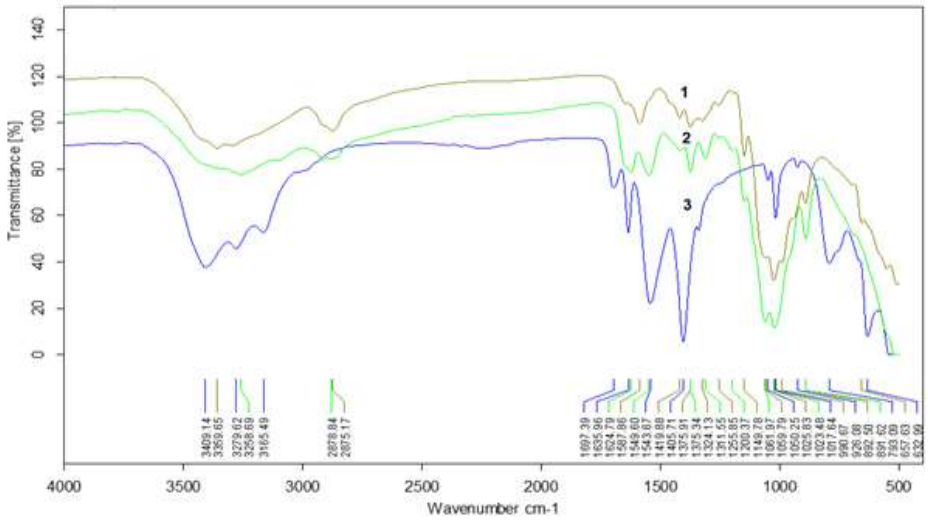

Figure 3. IR spectra of CS Bombyx mori (1), CSNA Bombyx mori (2) and AA (3).

Results of X-ray diffraction analysis. Comparative structural studies carried out using X-ray diffraction analysis are informative for the conversion of chitosan to nanoascorbate chitosan. From the data shown in Fig. 4, it can be seen that the diffraction patterns of chitosan and nanoascorbate chitosan have reflections of different intensity. In the case of nanoascorbate chitosan in the region of 2θ ≈ 10.3º, 20º, the reflections in the diffraction pattern do not have pronounced maxima and a sharp decrease in peaks at 2θ ≈10.3º, 20º is seen, which indicates a high degree of destruction of the supramolecular structure of nanoascorbate chitosan compared to initial chitosan, which may indicate the destruction of hydrogen bonds. The X-ray diffraction analysis results also confirm that during the formation of nanostructured ascorbate chitosan, the degree of crystallinity decreases due to sample amorphization. The results obtained are shown in figure 4, 5.

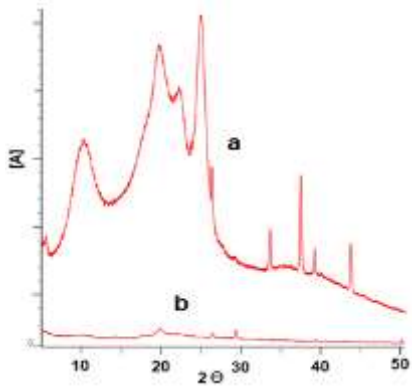

FIGURE 4. Results of XRD studies of samples of chitosan (a) and chitosan nanoascorbate (b).

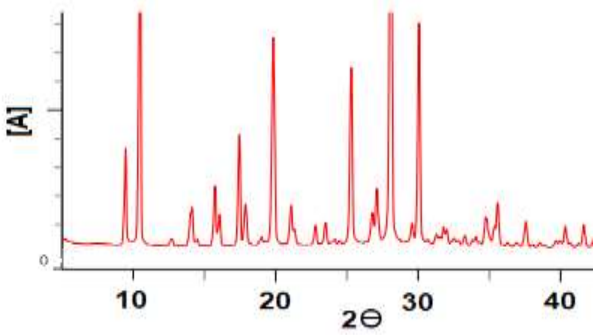

FIGURE 5. Results of X-ray diffraction studies of ascorbic acid samples.

It can be seen that in all samples obtained from the initial chitosan, characteristic reflections of the crystal structure of chitosan 2Ɵ from 10.3° to 27° are observed, associated with interlinear distances. In the obtained X-ray patterns of chitosan nanoascorbate, characteristic reflexes were revealed in the ranges 2Ɵ=10.3; 20.0; 30^0, inherent in the functional groups of acetamide, amine of chitosan and indicating a decrease in reflections for the crystal structure of the crystalline regions of the initial chitosan. Such changes in the crystal structures indicate the formation of chitosan nanoascorbate. On the diffraction patterns (fig. 5.) of ascorbic acid, characteristic crystalline peaks are observed at 2θ = 10.1, 15, 20, 25 and 30, which indicates the crystal structure of ascorbic acid due to the establishment of a hydrogen bond. Such characteristic reflexes are not founding on the X-ray patterns of CSNA, which can be attributing to the fact that the crystalline region of ascorbic acid is dispersed at the molecular level during the formation of chitosan nanoascorbate.

Results of quantum-chemical modeling

Model structures were built for simulating the possibility of structure of CSNA. Models presented as one unit of CS representing the main model molecule. The interactions between CS molecules with AA and TPP can occur, as observed in the results addressed so far, by hydrogen bonds involving -OH or $–NH_2$ groups from CS. To evaluate this interaction, as well as describe some quantum properties of CSNA model, which is scarce in the literature, a computational study was realized. To gain a deeper insight into the quantum properties of CSNA model are Frontier molecular orbital (FMO) were calculated. The FMO results provide knowledge about the energy gap and electronic properties between the HOMO and LUMO of the CS-AA and CS-TPP interactions. The HOMO can be considered the outermost orbital containing electrons, characterizes the ability to donor electron, while LUMO considered the innermost orbital containing free places to accept electrons [31].

The optimized structures of the CS-AA and CS-TPP interactions obtained at B3LYP/ 6-31++G(d,p) level of theory are shown in Figure 6. The distance between the hydrogen atom of the CS amino group and the oxygen atoms of nucleophiles is in the range of 1.52–1.98 Å, which is typical for hydrogen bonds and thus establishes the fact that the product of the interaction of one monomer units of CS with AA and TPP are held together by a hydrogen bond. A hydrogen bond is formed in the case of interaction of CS with AA (r = 1.60 Å, θ = 171.10), as well as CS with TPP (r = 1.53 Å, θ = 178.70). Usually a smaller θ value leads to a weaker hydrogen bonds [34]. According to calculations, the hydroxyl group of AA in position 3 (C3-O) will react with the amino group of CS, converting it into ammonium ions. The enol group of AA reacts with the $–NH_3^+$ group of CS with the formation of oxoammonium (Figure 1), due to the donor-acceptor interaction, a CS complex is formed. Amino groups in CS chains can be protonated by AA to form a positively charged water-soluble polysaccharide. CA in an acidic solution undergoes ionic gelation and forms CSA particles with a crosslinking agent added to the solution. Crosslinking occurs due to electrostatic interaction between positively charged amino groups of CS and negatively charged oxygen atoms of TPP. The size of the formed particle mainly depends on the concentration of the acid (acetic acid) and DD of CS [4, 6, 8, 16]. CS with a higher DD is characterized by a large number of effective binding points, i.e., amino groups that are protonated in an acidic solution [7]. Moreover, in an acidic solution, the degree of protonation of amino groups in the chains of CS increases, which, as a result, increases the ability to form cross-links with TPP. The binding of TPP to the polymer occurs until the degree of binding, which also depends on the concentration of TPP, decreases, which eventually leads to the formation of smaller nanoparticle sizes, and after saturation, excessive binding will lead to the formation of aggregates, resulting in a large particle size [2, 3, 7].

The magnitude of interaction is of paramount importance for nanostructure stabilization. A very strong or a feebly weak interaction, both are equally unfavorable for biological activity. A very weak interaction is unfavorable for the stability of such nanoparticles. For exhibiting biological activity, a suitable interaction energy range is 10 kcal/mol [13-17]. With an aim to examine the magnitude of interaction between CS and AA, TPP, we estimated the interaction energy using super molecular approach. Initially we calculated the interaction energies ($\Delta E_{int.}$) in gas phase and then observed the impact of aqueous phase on the interaction energy. In gas phase, $\Delta E_{int.}$ are observed to be quite high and the order is: CS-AA (-68.76 kcal/mol) > CS-TPP(-64.58 kcal). The observed trend does not corroborate with that predicted from the bond angle (θ) values in hydrogen bonding. This indicates that the bond angle in hydrogen bonding is not the sole criterion that governs the interaction energies between the two compounds.

During of CSNA delivery, transfection of nanoparticles takes place through a complex physiological medium, whose main constituent is water [10]. Cationic charge of CS attracts large scale of solvation and thereby enhances stability of CS. Therefore, incorporation of aqueous phase produces a spiky fall in interaction energies

as compared to gas phase. The aqueous phase $\Delta E_{int.}$ values of interactions are in the order: CS-AA (-13.67 kcal/mol) > CS-TPP (-11.2 kcal/mol). We have further calculated the free energy of solvation (ΔG_{sol}) of the chosen CS-AA and CS-TPP interactions using self-consistent reaction field theory [28]. The order is observed to be: CS-AA (-66.32 kcal/mol) > CS-TPP (-62.45 kcal/mol), higher ΔG_{sol} values are due to positive charge inherent in the interactions.

In the synergic effect of interactions of the type, $\mathrm{CS} + \mathrm{nucleophile(AA, TPP)} = \mathrm{CSNA}$, intermolecular hydrogen bond formation is favored when the HOMO of the CSNA has lower energy than the HOMO of CS or LUMO of AA and TPP [27]. Hence we have calculated the energy separation $\Delta E = (E_{HOMO,\ CSNA} - E_{HOMO,\ nucleophile\ (AA,\ TPP)})$, the calculated data show that E_{HOMO}, CSNA -7.43 eV (less than E_{HOMO}, nucleophile -9.63 eV and E_{LUMO}, CS -5.33 eV). This indicates that the formation of a hydrogen bond is beneficial in all considered interactions from the HOMO-LUMO energy data.

We observe quite high ΔE_{gas} values for CS-AA and CS-TPP interactions (-72.42 kcal/mol and -51.49 kcal/mol) in gas phase. Incorporation of aqueous phase lowers ΔE_{aq} values (-7.22 kcal/mol and -4.56 kcal/mol), respectively. However, no linear relationship between ΔE and ΔE_{int} is observed. Apart from ΔE values, shape of the LUMO of the donor and HOMO of the acceptor is also important. Figure 6 reveals that LUMO of CS-AA is localized over the $-NH_3^+$ group. Moreover, HOMO of CS-AA is spreading over on AA molecule, which makes them hydrogen acceptor during hydrogen bonding formation. The FMO of CS-TPP is localized over the TPP molecule, HOMO is slightly spreading over on $-NH_3^+$ group of CS molecule. To examine the thermodynamic driving force involved in the interactions we performed thermochemical analysis. The ΔG_{gas} and ΔG_{aq} values are presented in Table 3. It is evident that in gas phase, free energy favors interactions. In gas phase ΔG values follow the order CS-AA (-40.34 kcal/mol) < CS-TPP (-41.35 kcal/mol). However, a spiky fall in ΔG values is observed in aqueous phase exhibiting positive ΔG in most of the cases. ΔG_{aq} values are in the order: CS-AA (3.37 kcal/mol) < CS-TPP (3.08 kcal/mol). This clearly demonstrates the effect of solvent polarity on the parameter and denies the presence of any significant role of thermodynamic driving forces in aqueous phase.
In accordance with the literature data [14-16] and the data of the calculation results, we proposed a model of CSNA, is represented in Figure 7. Stability of the CSNA can be monitored in terms of global hardness, in both gas phase and aqueous phases. The result in Table 3 elucidates the gas and aqueous phase global hardness of CS-AA and CS-TPP. Global hardness of the interactions in both the phases are comparable but slightly higher values in aqueous phase implies that they are more stable in aqueous phase.

TABLE 3. Free energy, global hardness (in kcal/mol) in gas phase and aqueous phase of structures

Structure	ΔE_{gas}	ΔE_{aq}	ΔG_{gas}	ΔG_{aq}	η, gas phase	η, aqueous phase
CS-AA	- 72.42	-6.82	-40.34	3.37	63.7	60.3
CS-TPP	- 51.49	-4.56	-41.35	3.08	49.7	59.3

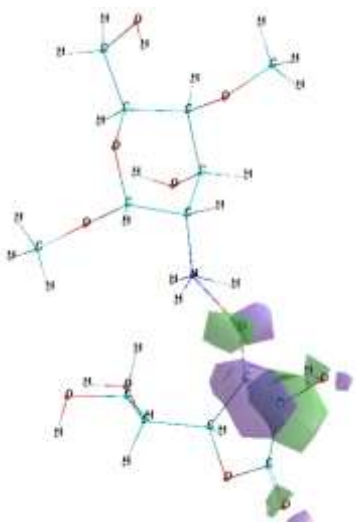

HOMO of CS-AA

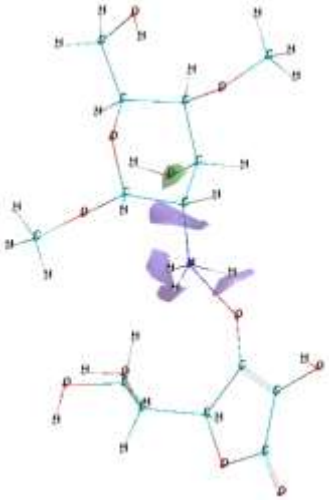

LUMO of CS-AA

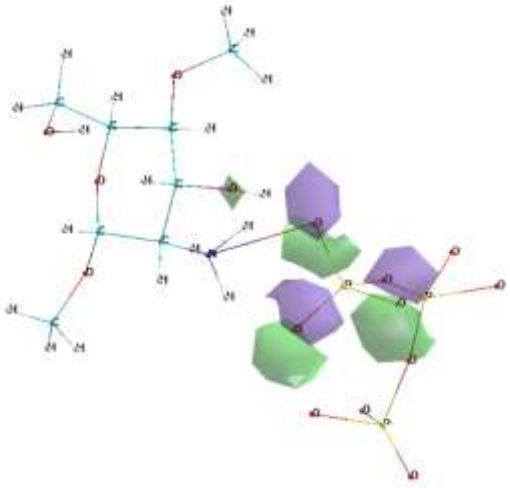

HOMO of CS-TPP

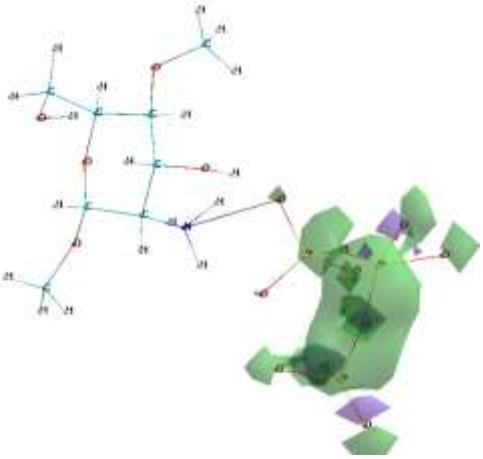

LUMO of CS-TPP

FIGURE 6. Molecular orbital surfaces for HOMO and LUMO of CS-AA and CS-TPP.

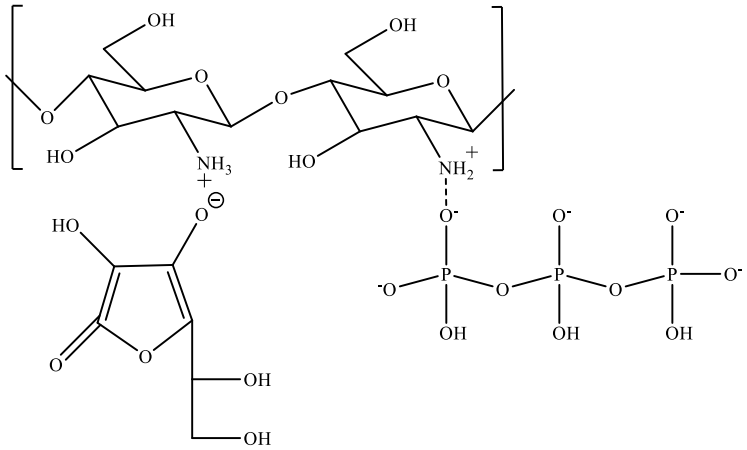

FIGURE 7. Interaction mechanism of CS-AA-TPP.

5. Conclusions

Thus, the synthesis of CSNA based on Bombyx mori CS was carried out for the first time and the physicochemical properties were determined using IR spectroscopic methods. The particle size of CSNA Bombyx mori was estimated by electron microscopy. The results obtained confirm that the particle size of CSNA is on average 16–100 nm. The values of the reaction orders for CS and AA were determined which are equal to 0.5–0.9, indicating that in the formation of CSNA per unit time there are twice as many molecules of AA as compared to CS molecules.
DFT: B3LYP/6-31G (d,p) model was used to study the ability of CS to interact with AA and TPP for the nanostructure formation. The DFT results establish the existence of strong hydrogen bonding between CS and the AA and TPP in gas phase. The incorporation of the aqueous phase resulted fall in interaction energy between the two molecules. The introduction of the aqueous phase led to a drop in the interaction energy. In addition, an increase in the acidity of the medium, the concentration of AA and TPP as well as the DD of CS can be considered as a tool for obtaining nanoparticles of various sizes. CS nanoparticles can protect AA from degradation and improve the stability of AA. The introduction of the aqueous phase led to a drop in the interaction energy. CS-based drug delivery systems can be improved by adopting different theoretical and synthetic techniques and selecting appropriate process parameters and functional properties.

6. References

1. Milusheva, R. Yu., Rashidova, S. Sh. Bombyx Mori Chitosan Nanoparticles: Synthesis and Properties (2019) Open Journal of Organic Polymer Materials, **9**, 63-73.
2. Alishahi, A., Mirvaghefi, A. (2011) Shelf life and delivery enhancement of vitamin C using chitosan nanoparticles. Food chemistry, **126**, 935–940.
3. Altınışık, A.T., Sarp, Ö., Yurdakoç, K. (2018) Controlled Release of Vitamin C from Chitosan Nanoparticles. Hacettepe Journal of Biology and Chemistry, **46**. 69-77.
4. Pirniyazov, K.K. Rashidova, S. Sh. (2019) Synthesis and structural characteristics of the ascorbat chitosan Bombyx mori. American Journal of Research, **7-8**, 114-119.
5. Baek, J., Ramasamy, M., Carly Willis, N., Kim, D. S., Anderson, W. A., Tam, K. C. (2021) Encapsulation and controlled release of vitamin C in modified cellulose nanocrystal/chitosan nanocapsules. Current Research in Food Science, **4**, 215–223.
6. Pirniyazov, K. K., Rashidova, S. Sh. (2020) Synthesis of ascorbate and nanoascorbate of chitosan and their biologically active properties. Science and innovative development, **5**, 47–62.
7. Tian, D. F. Tian, Z. Y. Wang, F. K. Mo (2009) Synthesis and Evaluation of Chitosan-Vitamin C Complex. Indian Journal of Pharmaceutical Sciences, **71**, 371–376.
8. Pirniyazov, K. K., Tixonov, V. E., Rashidova, S. Sh. (2021) Oligochitosan and Oligochitosan Ascorbat: Preparation and Properties. International Journal of Modern Agriculture, **10,** 1244–1262.
9. Gegel'a, N. O., Zudina, I. V., Malinkina, O. N., Shipovskaya A. B. (2018) Effect of Ascorbic Acid Isomeric Forms on Antibacterial Activity of Its Chitosan Salts. Microbiology, **87**, 732–737.
10. Rossi, S., Vigani, B., Puccio, A., Bonferoni M. C., Sandri, G., Ferrari, F. (2017) Chitosan ascorbate nanoparticles for the vaginal delivery of antibiotic drugs in atrophic vaginitis. Marine Drugs, **15**, 319–320.
11. Pirniyazov, K. K., Rashidova, S. Sh. (2020) Study of the kinetics of Bombyx mori chitosan ascorbate formation. Bulletin of the Karaganda University. Chemistry series, **3**, 38–43.
12. Sekar, V., Rajendran, K., Vallinayagam, S., Deepak, V., Mahadevan S. (2018) Synthesis and characterization of chitosan ascorbate nanoparticles for therapeutic inhibition for cervical cancer and their in silico modeling. Journal of Industrial and Engineering Chemistry, **62.** 239–249.
13. Fan, W., Yan, W., Xu, Z., Ni, H. (2021) Formation mechanism of monodisperse, low molecular weight chitosan nanoparticles by ionic gelation technique. Colloids and Surfaces B: Biointerfaces, **90**, 21–27.
14. Nuri, A.E. (2021) Formulation and characterization of ascorbic acid nanoparticle with chitosan as a carrier for topical administration. Proceeding of International Conference on Drug Development of Natural Resources, 317–321.
15. Othman, N., Masarudin, M. J., Kuen, C. Y., Dasuan, N. A., L. C. Abdullah, Ain Md Jamil, S. N. (2018) Synthesis and optimization of chitosan nanoparticles loaded with L-ascorbic acid and Thymoquinone. Nanomaterials, **8**, 920.
16. Santosh, K., Joonseok, K. (2012) Physiochemical, optical and biological activity of chitosan-chromone derivative for biomedical applications. International Journal of Molecular Sciences, **13**, 6102–6116.

17. Frisch M. J., Trucks G. W., Schlegel H. B., Scuseria G. E., Robb M. A., Cheeseman J. R., Scalmani G., Barone V., Mennucci B., Petersson G.A., et al., (2010) Gaussian, Inc., Wallingford CT.
18. Becke, A.D. (1993) Density-functional thermochemistry. III. The role of exact exchange. The Journal of Chemical Physic, **98**, 5648-5652.
19. Lee, C., Yang. W., Parr. R. G. (1988) Development of the Colle-Salvetti correlation-energy formula into a functional of the electron density. Physical Review B., **37**, 785-789.
20. Miehlich, B., Savin, A., Stoll, H., Preuss, H. (1989) Results obtained with the correlation energy density functionals of becke and Lee, Yang and Parr. Chemical Physics Letters, **157**, 200-206.
21. Krishnan, R., Binkley, J. S., Seeger, R., Pople, J. A. (1980) Self-consistent molecular orbital methods. XX. A basis set for correlated wave functions. The Journal of Chemical Physics, **72**, 650.
22. Parr, R. G., Yang, W. (1984) Density functional approach to the frontier-electron theory of chemical reactivity. Journal of the American Chemical Society, **106**, 4049–4050.
23. Chandrakumar, K. R. S., Pal, S. (2002) The concept of density functional theory based descriptors and its relation with the reactivity of molecular systems: a semi quantitative study, International Journal of Molecular Sciences, **3**, 324–337.
24. Koopmans, T. (1934) Über Die Zuordnung Von Wellenfunktionen Und Eigenwerten Zu Den Einzelnen Elektronen Eines Atoms. Physica, **1**, 104-113.
25. Marenich, V., Cramer, C. J., Truhlar, D. G. (2009) Universal solvation model based on solute electron density and a continuum model of the solvent defined by the bulk dielectric constant and atomic surface tensions. The Journal of Physical Chemistry B, **113**, 6378–6396.
26. Mennucci, B., Tomasi, J. (1997) Continuum solvation models: a new approach to the problem of solute's charge distribution and cavity boundaries. The Journal of Chemical Physics, **106**, 5151–5198.
27. Mennucci, B. (2012). Polarizable continuum model. Wiley interdisciplinary reviews: Computational Molecular Science, **2**, 386-404.
28. Chalasinski, G., Szczesniak, M.M. (1994) Origins of structure and energetics of van der Waals clusters from ab initio calculations. Chemical Reviews, **94**, 1723–1765.
29. Galano, A., Idaboy, J. R. A. (2006) A new approach to counterpoise correction to BSSE. Journal of Computational Chemistry, 27, 1203–1210.
30. Ozdemir, M.C., Ozgün, B., Aktan, E. (2019) 1-Aryl-3,5-dimethylpyrazolium based tunable protic ionic liquids (TPILs). Journal of Molecular Structure, **1180**, 564-572.
31. Ireta, J., Neugebauer, J., Scheffler, M. (2004) On the accuracy of DFT for describing hydrogen bonds; dependence on the bond directionality. The Journal of Physical Chemistry A, **108**, 5692–5699.